JOURNAL OF MATERIALS SCIENCE **34** (1999) 3203–3211

Characterization of single and discretely-stepped electro-composite coatings of nickel-alumina

S. W. BANOVIC, K. BARMAK, A. R. MARDER
Department of Materials Science and Engineering, Lehigh University, Bethlehem, PA 18015, USA
E-mail: swb0@lehigh.edu

Electrodeposition from a sulfamate bath has been used to produce single layer and discretely stepped electro-composites consisting of a metallic nickel matrix with second phase alumina (α-Al_2O_3) particles. Light optical microscopy (LOM), scanning electron microscopy (SEM), quantitative image analysis (QIA), and micro-indentation techniques were used to characterize the deposits. As previously seen, an increase in bath particle loading and decrease in plating current density increased the volume percent of alumina incorporated into the coating, with a maximum of 40 vol % being attained. For samples deposited above 1 A/dm^2, a direct relationship between the alumina volume percent and coating hardness was seen due in part to the related decrease in interparticle spacing (IPS) at the higher vol %. However, the strengthening mechanism of the electro-composites may be more complex with both the metallic nickel grain structure and IPS being factors, as seen for samples deposited at 0.5 A/dm^2. The incorporation of alumina into the electrodeposited nickel was also observed to affect the as-plated surface structure of the coating. Due to the particles inhibiting the formation of pyramidal features found on the surface of pure nickel electrodeposits, the electro-composite surfaces were observed to be relatively flat. Also, structure within the metallic nickel matrix appeared due to rapid growth of the nickel coating around the inert particles when plated at high current densities. In addition, discretely layered functionally graded materials were produced without alterations to the original deposition procedure of the single layer deposits. It was found that the various processing stages needed to produce the stepped coatings did not affect the structure or properties of the individual layers, when compared to that of the corresponding single-layered electro-composites.

1. Introduction

Graded coatings have been produced by various methods such as thermal plasma spray [1, 2], physical vapor deposition [3], chemical vapor deposition [4–8], and electro-deposition [9–12]. Processing drawbacks such as restrictions on size or shape of the component being coated currently limit the first three methods [13]. Electro-deposition, however, is a fabrication technique that combines the ability to deposit on both complex shapes and large sizes with the advantages of low cost of equipment and raw materials and production at ambient temperature and pressure. In addition, changing the volume percent inert particle in the electro-deposited coating, critical to producing graded materials, can easily be accomplished through manipulation of processing parameters [9–11, 14–21]. This was observed by varying the current density and particle loading in the bath [9]. Plated from a sulfamate electrolyte solution, both single layer and discretely-stepped electro-composites were produced that consisted of a co-deposited metallic nickel matrix with second phase α-alumina particles (Ni-Al_2O_3). The single layers were relatively uniform and contained well dispersed particulates with a maximum of 40 vol % alumina. Further, discretely-stepped, layered electro-composites were produced with the same relative ease without modification to the deposition process. The objective of this paper is to further characterize these nickel-alumina electro-composites coatings, both homogeneous single layer and discretely-stepped, using microscopy and quantitative image analysis techniques. In addition, the mechanical property of hardness is investigated and related to the structure of the deposits.

2. Experimental

The sulfamate bath composition and parameters used for deposition can be found in Table I. The current density was varied from 0.5 to 25 A/dm^2 with bath loadings of 75, 150, and 225 g/l of α-alumina particles. Their average size was 0.6–0.8 μm. Details of the deposition procedure are reported elsewhere [9].

Following deposition, samples for microstructural characterization and cross-sectional micro-indentation

tests were sectioned with a low speed diamond saw and mounted in cold setting epoxy. The samples were ground to 1200 grit finish with silicon carbide papers and polished to 0.05 μm colloidal silica using standard metallographic procedures. To observe coating microstructure, a solution of 25% water, 25% acetic acid, and 50% nitric acid was used as an etchant.

Deposit microstructures were characterized through use of light optical microscopy (LOM) and scanning electron microscopy (SEM). Relative reflectivity of the sample surfaces was measured by interfacing an Olympus Exposure Control unit, used to determine the exposure time for photography, with a light optical microscope. A polished substrate was focused and the light intensity set so that the exposure time indicated 1.0 seconds. Without re-adjusting the intensity, sample surfaces were then focused and the exposure time recorded. An increase in exposure time indicated that less light was received by the detector, and hence, a rougher surface.

The volume percent of alumina incorporated into the coating was determined through quantitative image analysis (QIA). This was conducted using a LECO 2001 image analyzer. Coating thickness was measured using a digitizing pad interfaced with a light microscope and interparticle spacing was determined by the mean linear intercept method on scanning electron micrographs. Microhardness measurements were conducted on polished cross-sections of the coatings in accordance with ASTM standard E-384. A Knoop indenter was used with a load of 100 g held for 15 seconds. Averages were calculated from 15 to 20 measurements per sample.

TABLE I Electrolyte bath composition and process parameters

Sulfamate bath composition
400 g/l Nickel sulfamate tetrahydrate [$Ni(NH_2SO_3)_2 \cdot 4H_2O$]
30 g/l Boric acid powder [H_3BO_3]
5 g/l Nickel (II) chloride hexahydrate [$NiCl_2 \cdot 6H_2O$]
0.5 g/l Sodium laurel sulfate [$(CH_3(CH_2)_{10}CH_2OSO_3Na$]
0.1 g/l Coumarin [$C_6H_4OCOCHCH$]
Temperature: 50 °C ± 2 °C
pH: 4.0 ± 0.3
Mechanically agitated at 400 rpm

3. Results and discussion

3.1. Single layer deposits

3.1.1. Structure

Some of the as-plated surfaces of the electrocomposites are shown in Fig. 1. Overall, they are relatively flat with entrapped alumina particles on the surface. In some areas, holes can be seen in the matrix, presumably from partially entrapped particles losing adhesion and falling out of the coating subsequent to deposition. For samples deposited below 1 A/dm^2, the nickel matrix was relatively smooth, while above this current density, some structure can be observed within the matrix (arrows in Fig. 1d and f). This structure within the matrix is attributed to the growth and coalescence of the depositing nickel around the particles. Since the alumina particles are inert, the nickel matrix can not plate onto them, but instead, must plate around them. Therefore, it is the difference in the rate of coalescence of the depositing nickel layer on top of the particle at the various current densities that gives this appearance, as schematically illustrated in Fig. 2. At the higher current densities, the nickel adatoms are being incorporated faster than they can diffuse across the surface. This results in growth of nickel around the particle becoming rough and the formation of a ridge, as seen schematically in Fig. 2c and experimentally in Fig. 1d and f. At the lower current densities, the coating deposits at a much slower rate, thus allowing surface

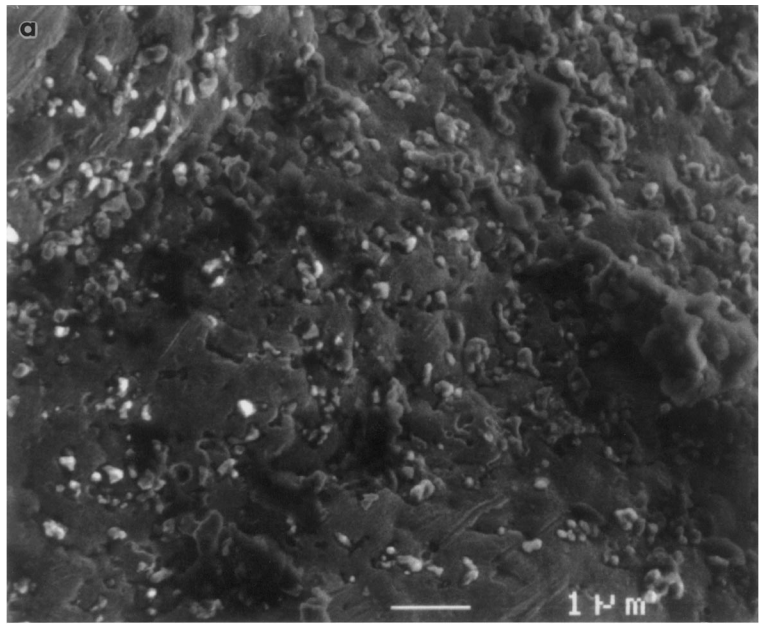

Figure 1 (a, b) SEM micrographs of the as-plated electro-composite surfaces showing the relatively smooth nickel matrix of the samples deposited at 0.5 A/dm^2. (c, d) SEM micrographs of the as-plated electro-composite surfaces showing some structure in the nickel matrix due to fast growth of the coating. Samples deposited at 5 A/dm^2. (e, f) SEM micrographs of the as-plated electro-composite surfaces showing some structure in the nickel matrix due to fast growth of the coating. Samples deposited at 20 A/dm^2. (*Continued*).

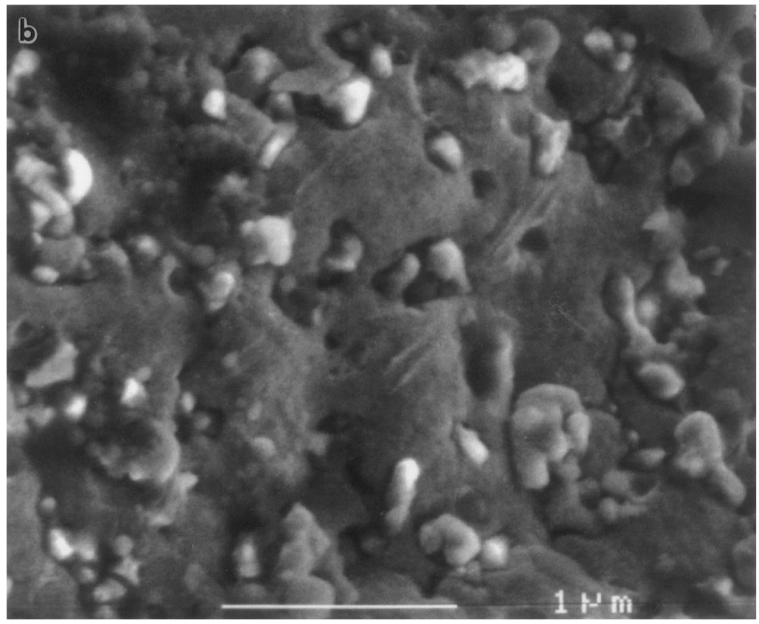

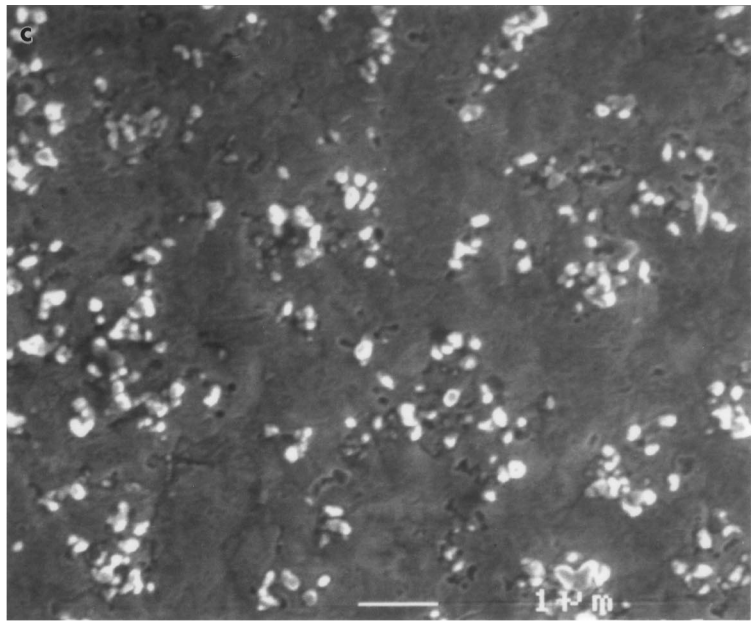

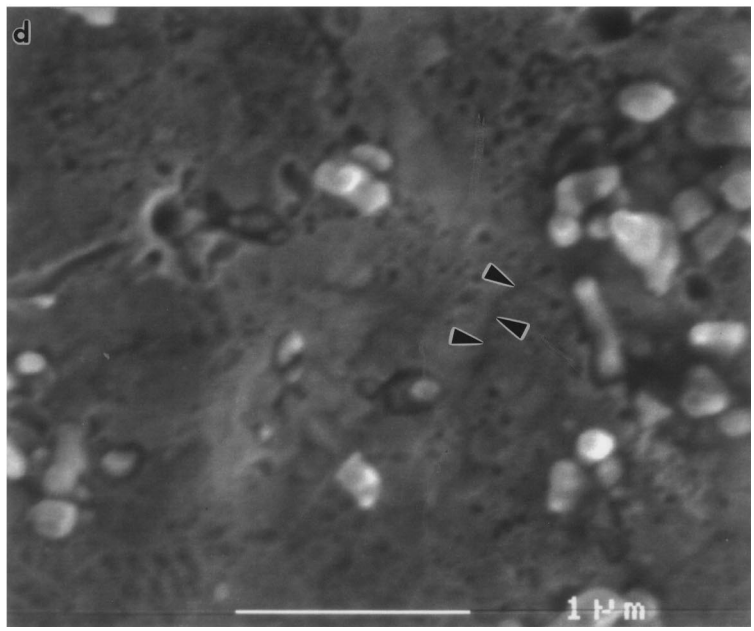

Figure 1 (*Continued*)

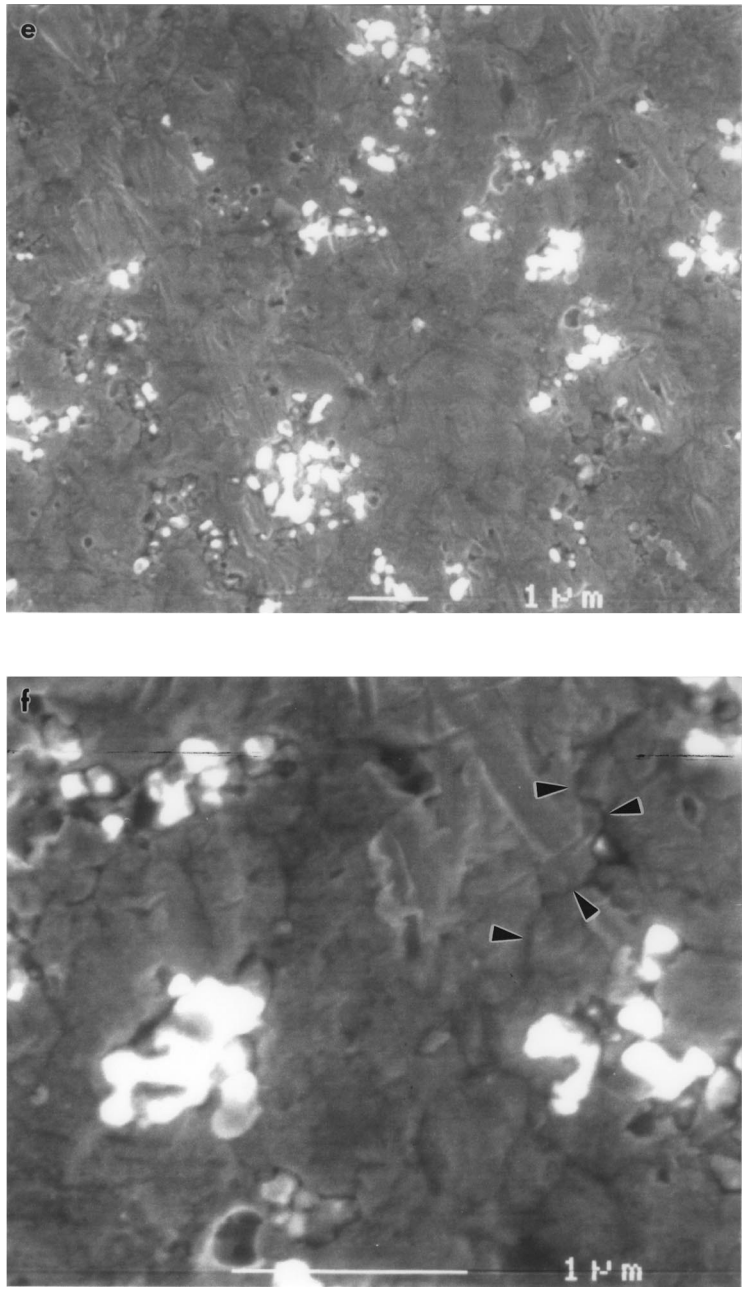

Figure 1 (*Continued*).

diffusion to occur and a smoother appearance to be attained, Figs. 1b and 2f.

Missing from the electro-composite surfaces are the pyramidal features found on the surface of the nickel electrodeposits [22]. These structures were observed to grow on favorably oriented crystals in order to give the fastest growth rates [23–25]. With an increase in current density, an increase in the size of the structures was seen both visually and through their relative reflectivity measurements. Fig. 3 shows these measurements for as-plated and polished electro-composites, as well as the nickel electrodeposits. With an increase in the exposure time, less light is being detected, indicating a decrease in the reflectivity of the sample and a rougher surface. As-plated, the electro-composites are seen to have a higher exposure time than the pure nickel samples deposited between 0.5 and 10 A/dm^2. This effect was attributed to the roughening of the surface due to particle incorporation, in conjunction with the particles on the surface. By contrast, for samples deposited from 15 to 25 A/dm^2, the exposure time is lower than that for the pure nickel deposits, even with particles on the surface. The incorporated alumina was seen to inhibit the growth of the pyramidal shapes, and hence, produce a relatively flatter surface when compared to the nickel electrodeposits of the corresponding current density. Also, the volume percent of particles incorporated into the coating had only a minor effect on the reflectivity. As seen from the polished surfaces, only a slight increase in exposure time was noted for an increase in volume fraction of particles incorporated. Therefore, it is assumed that it is the particles' effect on the pyramidal growths of the coating that caused the change in exposure time.

Typical light optical micrographs of polished electro-composite cross-sections can be seen in Fig. 4. The

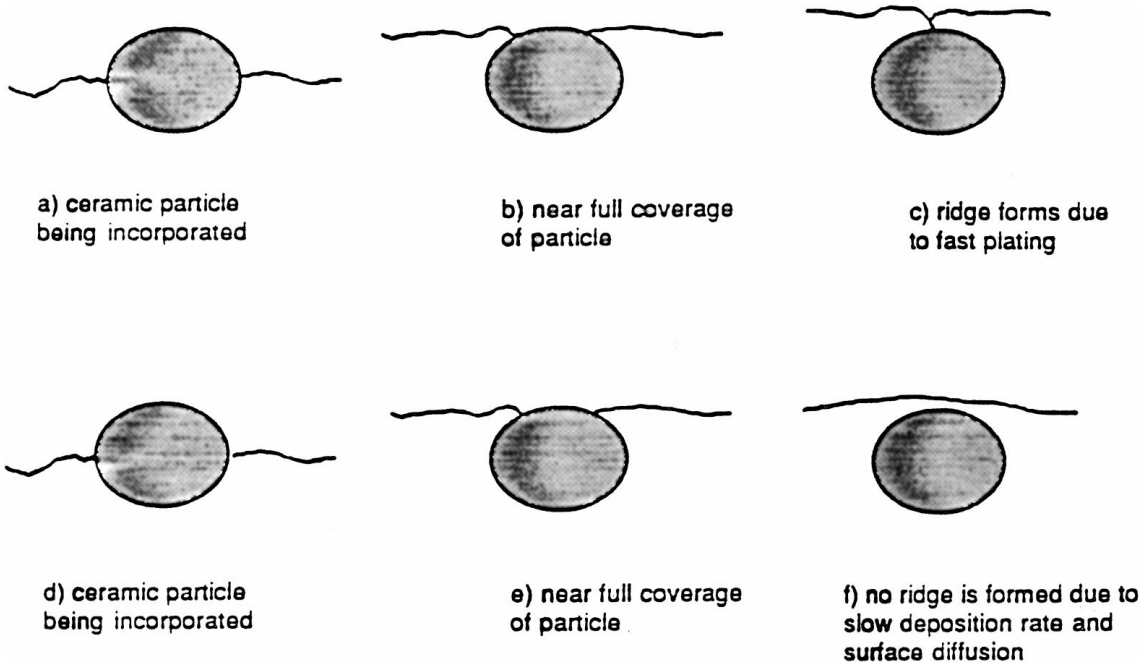

Figure 2 Schematic illustrating the different surface morphologies of the electro-composites deposited at different current densities. A high plating rate (current density) is observed in (a), (b), and (c). A slower plating rate is found in (d), (e), and (f).

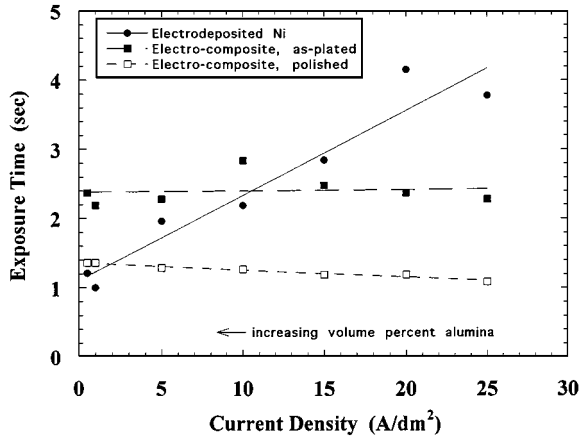

Figure 3 The relative surface reflectivity for both sets of electro-composites and electro-deposited nickel as a function of current density indicated by exposure time.

microstructures reveal a relatively uniform distribution of alumina within the matrix. Agglomeration of the particles was observed and found to have an average "cluster" size of approximately 1 μm. Etching of the matrix structure proved difficult because the etchant preferentially attacked the interface between the ceramic particle and the matrix, thus suppressing the grain structure. A similar effect was observed by Greco and Baldauf [14]. Nickel electro-deposits showed columnar grains in cross-section for samples deposited above 1 A/dm^2 [9, 22]. The grain widths were observed to increase with current density, Fig. 5. However, it is not clear if a similar trend will be found in the electro-composites, as the existing evidence in the literature shows contradictory behavior. For example, transmission electron microscopy (TEM) analysis [10] showed that the presence of alumina particles did not produce a strong global change in the nickel matrix grain size. Thus, the electro-composites will have similar columnar grain widths when compared to corresponding nickel electrodeposits. In contrast to these observations, Hayashi, Maeda, and Furukawa [15] found that the addition of alumina particles effectively refined the nickel matrix grain size. Their method of analysis was through LOM, but no micrographs were provided. Finally, Bazzard and Bowden [26] suggested that incorporation of inert particles will increase the local cathode current density, resulting in an increase in the matrix grain size.

The amount of incorporated alumina increased with a decrease of plating current density and increased bath loading, Fig. 6. This finding was in agreement with that found by other researchers [9–11, 14–21] who proposed that increasing the number of effective collisions between the particles and the cathode surface per unit volume of deposited matrix will increase the amount incorporated into the coating. This can be accomplished by using a slower plating rate, i.e. lower current density, or increasing the number of particles suspended in the electrolyte. With a change in the volume percent of particles in the coating, it is expected that a concomitant change in the interparticle spacing will occur, providing the particle size does not change. Fig. 7 shows the interparticle spacing of the samples as a function of the inverse square root of the volume percent. The closed circles represent the spacing as obtained using the linear intercept method on scanning electron micrographs of the coatings. The open circles represent the spacing as obtained from LeRoy's Equation [27]

$$\mathrm{IPS} = (0.77 \cdot d)/v_{\mathrm{f}}^{1/2}$$

where d is the average agglomeration size of the alumina particles and v_{f} is the volume percent alumina in the coating. The results obtained for both methods are similar.

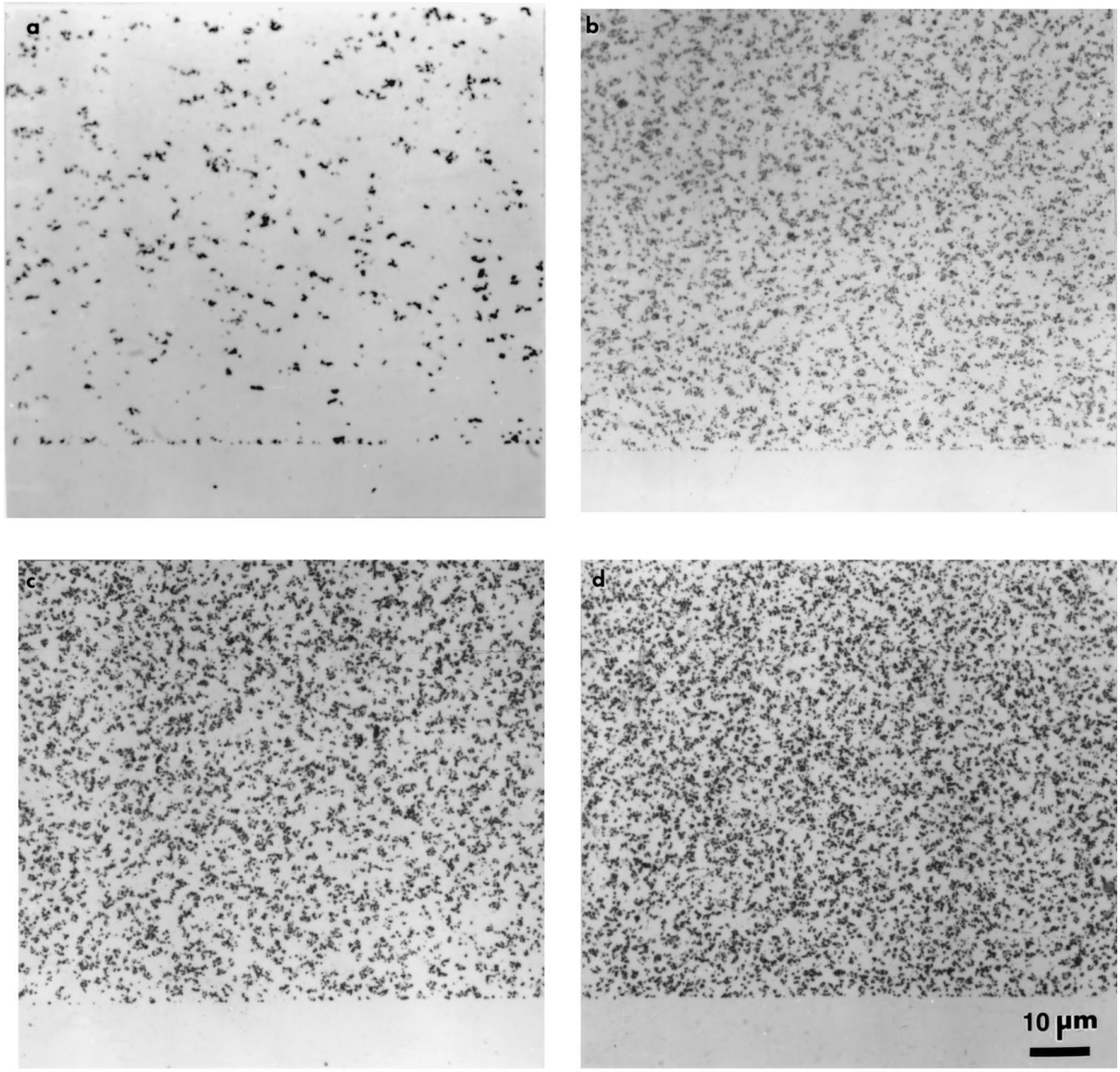

Figure 4 LOM micrographs of the polished cross-sections of various electro-composite samples showing the changing volume percent of alumina. (a) 4.1, (b) 16.6, (c) 32.8 and (d) 38.9 vol %.

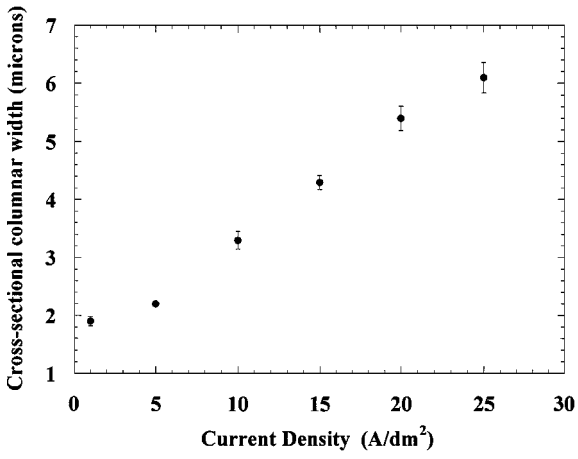

Figure 5 Cross-sectional columnar grain width as a function of the plating current density for electro-deposited nickel.

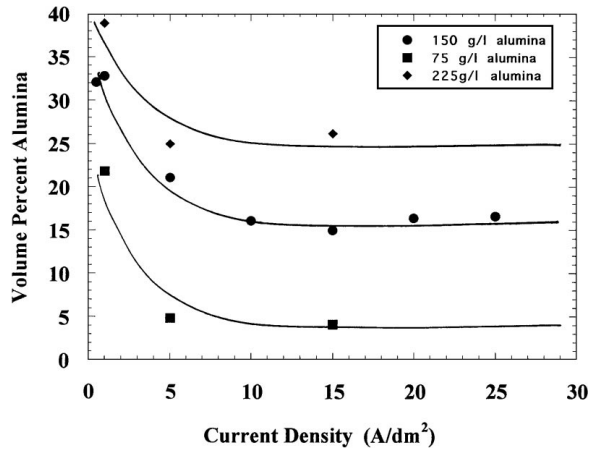

Figure 6 Volume percent alumina incorporated as a function of current density and bath loading.

3.1.2. Properties

Fig. 8 shows the hardness of the electro-composites as a function of the current density and bath loading. It can be seen that there is a concomitant increase in the hardness with increased volume percent alumina in the coating. This is due to the rigid particles inhibiting plastic flow of the softer matrix. Assuming that the inert particles did not affect the microstructure of the deposits, i.e. increase/decrease the columnar grain widths, the columnar grain widths will be larger than

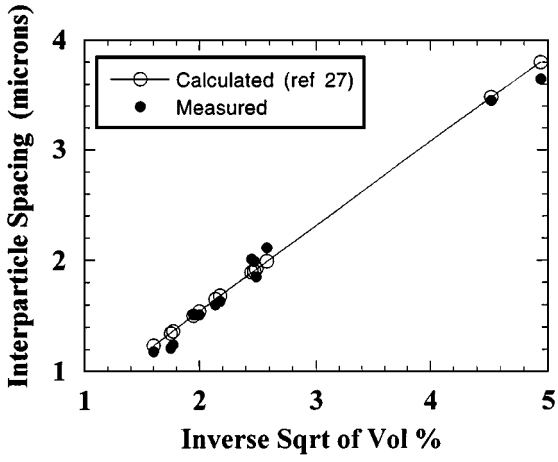

Figure 7 Interparticle spacing (IPS) as a function of volume percent alumina incorporated. Measured values show good agreement with calculated ones.

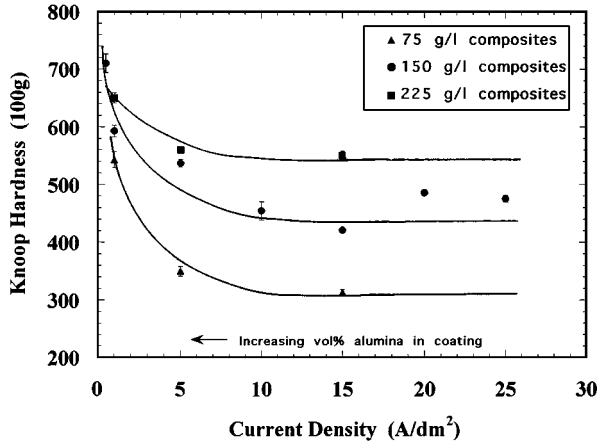

Figure 8 Knoop hardness as a function of current density and bath loading.

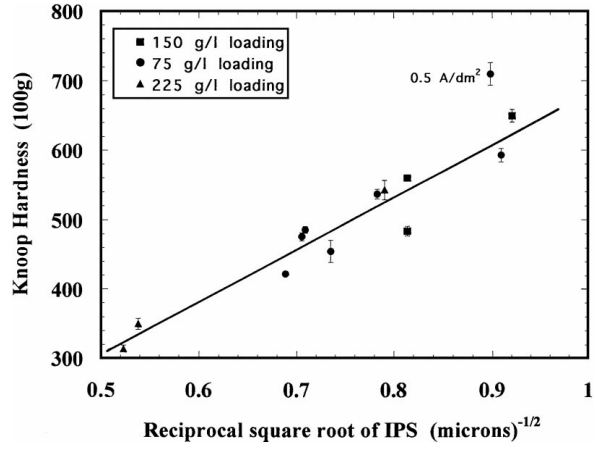

Figure 9 Hardness as a function of the reciprocal square root of the IPS showing a relationship exists between the two.

the distance between the incorporated alumina particles. Therefore, it might be expected that the interparticle spacing (IPS) is the controlling length scale with regards to the hardness. Fig. 9 shows this correlation exists. However, the data does not extrapolate to the correct hardness for pure nickel electrodeposits. One possible explanation is that the hardening produced in the composites is not caused entirely by the dispersed particles, but additional factors may have arisen from the nickel matrix grain structure being altered.

A case for this may be made by examining the volume percent of alumina incorporated and the corresponding hardness measurements of various samples. At 1 A/dm^2 with 225 g/l alumina in the electrolyte solution, samples were produced with approximately 40 vol % alumina and a resulting hardness of 650 HKN. However, samples deposited at 0.5 A/dm^2 with a bath loading of 150 g/l attained a hardness of 710 HKN with only 32 vol % alumina in the deposit. This increased hardness may be attributed to the difference in structure of the deposited nickel matrix. It has previously been shown that at this relatively low current density (0.5 A/dm^2), a banded or laminar type structure was seen in cross-section for the nickel electrodeposits, as compared to the columnar grains found for the higher current densities [22]. The strengthening mechanism of this nickel deposit was unresolved, but believed to be due in part to a combination of finer grain size, as well as the incorporation of foreign ions plated into the coating that occurs at these lower current densities. A similar strengthening may also be present for the nickel-alumina electro-composites plated at 0.5 A/dm^2. Fig. 9 also shows this ambiguity as the samples plated at 0.5 A/dm^2 do not comply with the relationship between hardness and IPS. Therefore, a more complex relationship may exist for the strengthening mechanism of the electro-composites, with both the IPS and grain size being factors.

3.2. Graded electro-composites

3.2.1. Structure

Through manipulation of processing variables, discretely graded electro-composites, with layers of varying volume percent of alumina, were produced. Table II shows a summary of the processing variables for the stepped composite. A characteristic micrograph of the as-plated cross-section can be seen in Fig. 10. The structure consists of an inner, pure nickel layer and two electro-composite layers with increasing volume percent of alumina (15 and 30%). Table III summarizes the results obtained from the processing of the stepped structure. As observed, the deposition rates for the individual layers were not affected by the various fabrications steps and the layer thickness measurements were in good agreement with those specified prior to deposition. In addition, the incorporation of alumina particles was not influenced by the change in processing

TABLE II Electrodeposition parameters for stepped structures

Field	Current density (A/dm^2)	Bath loading (g/l)	Deposition time (min)
1	15	0	25
2	15	150	25
3	0.5	150	480

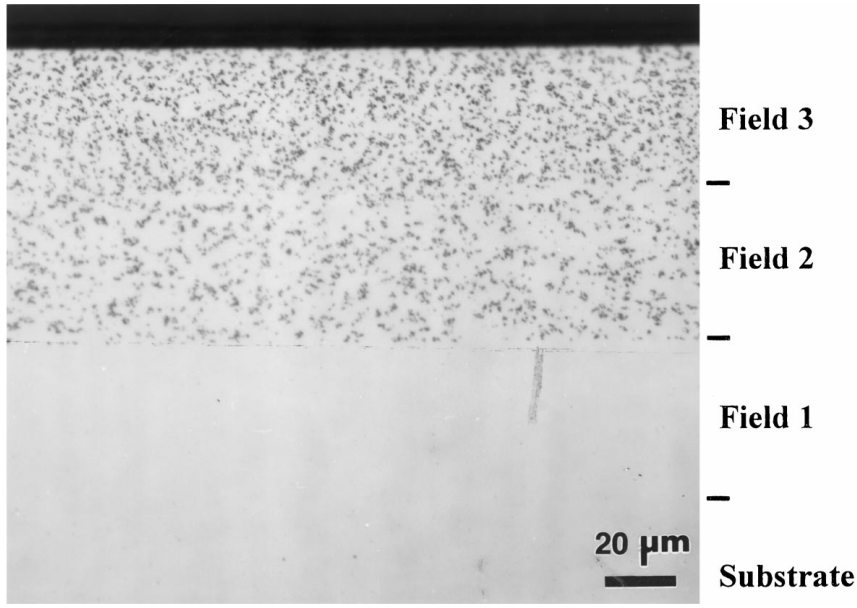

Figure 10 Light optical micrograph of a polished cross-section of a stepped electro-composite coating.

TABLE III Summary of measurements for the stepped coating

Field	Aim thickness (μm)	Measured thickness (μm)	Aim volume %	Measured volume %
1	40	39 ± 2.8	0	0
2	40	43 ± 3.2	15	14.6 ± 0.7
3	40	45 ± 5.1	30	33.1 ± 1.2

TABLE IV Summary of microhardness for stepped coatings

Field	Expected HKN	Measured HKN
1	293	301 ± 9
2	422	427 ± 8
3	710	703 ± 11

conditions. A visible interface between the individually deposited layers was not observed on the as-plated structure, Fig. 10. However, the interfaces can be seen to be linear in the etched microstructure (Fig. 11). By observing the interface between the pure nickel coating and the composite layer containing 15 vol %, it appears that the columnar structure is continuous from one layer to the next. The structure of the interface between the two composite layers could not be observed due to the poor etch of the higher volume percent deposit.

3.2.2. Properties

Fig. 12 shows the characteristic hardness profile of the discretely graded structure. The hardness of the homogeneous single electroplates and the corresponding layer within the stepped-structure are in good agreement (Table IV). This suggests that the microstructures and properties of the individual layers have not been altered in producing the stepped composites.

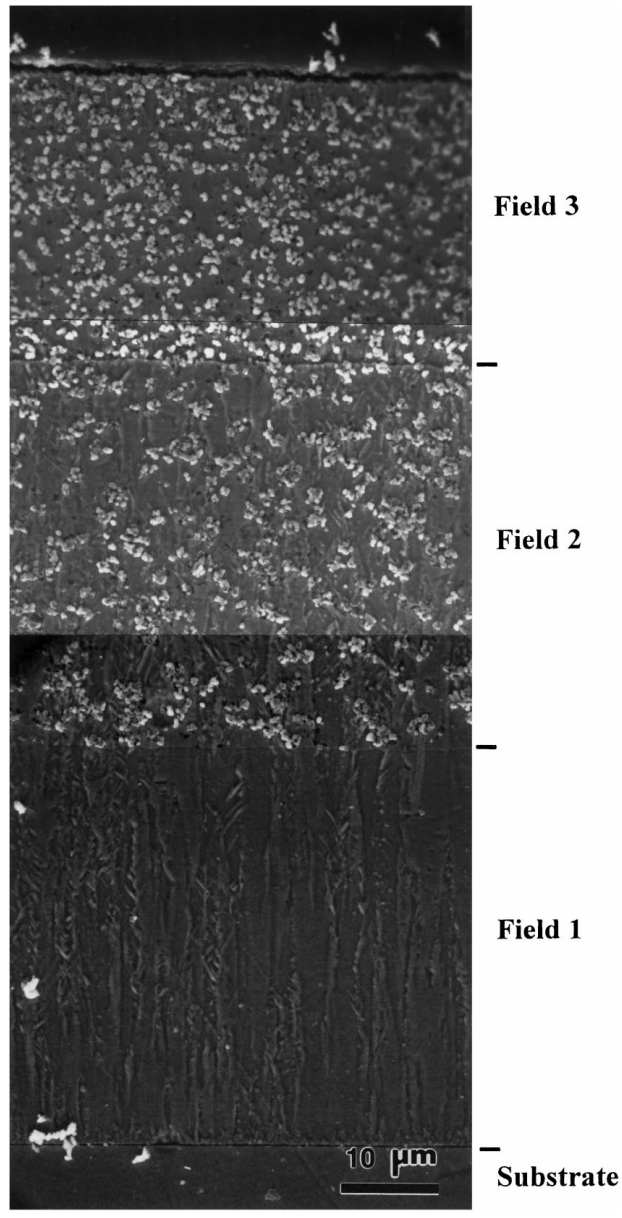

Figure 11 Scanning electron micrograph of an etched cross-section of a stepped coating.

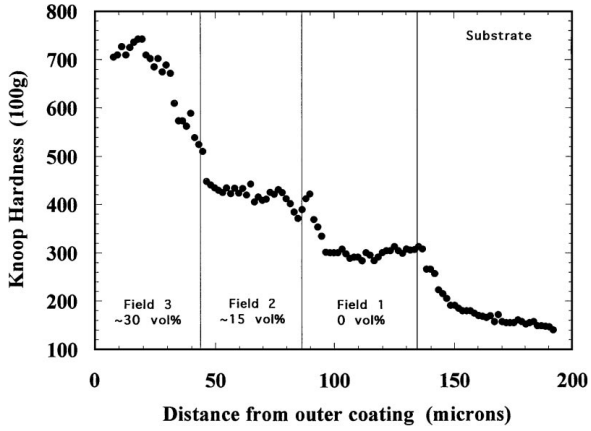

Figure 12 Knoop hardness profile for a stepped electro-composite.

4. Summary

Single layer and discretely-stepped electro-composite coatings were produced from a sulfamate bath. The platings consisted of a co-deposited metallic nickel matrix with second phase alumina particles. As previously seen, the volume percent of alumina incorporated into the coating was observed to increase with an increase in bath particle loading and decrease in current density. This increase in volume percent of alumina led to a decrease in interparticle spacing and a concomitant increase in the coating hardness. However, the strengthening mechanism of the deposits may have a more complex relationship with both the metallic nickel grain structure and IPS being factors. The incorporation of alumina into the electro-deposited nickel was also observed to affect the structure of the coating. The formation of pyramidal features found on the surface of pure nickel electro-deposits was inhibited due to the incorporated alumina, thus causing the electro-composites to be relatively flat. Also, when plated at high rates, structure within the metallic nickel matrix on the as-plated surfaces appeared due to rapid growth of the nickel coating around the inert particles. In addition to the single layered electro-composites, discretely layered functionally graded materials were also produced without altering the original deposition procedure from the single layer deposits. The structure and properties of the individual layers within the coating, when compared to the single layer coatings, were not affected by the different processing techniques.

Acknowledgements

This work was made possible by the research subcontract DE-FC21-92MC29061 sponsored by the U.S. Department of Energy—Morgantown Energy Technology Center through a cooperative agreement with the South Carolina Energy Research Development Center at Clemson University. S. W. Banovic thanks the National Science Foundation for financial support through Graduate Traineeships in Materials Science and Engineering, DMR-9256332. C. M. Petronis is recognized for her help in preparation of some of the samples. R. Chaim is acknowledged for helpful discussions. Microstructural observations reported here would not have been possible without the aid of A. O. Benscoter.

References

1. D. A. JAGER, D. STOVER and H. G. SCHULTZ, in Proc. 4th National Thermal Spray Conference, edited by T. F. Bernecki (ASM International, Materials Park, OH, 1991) pp. 323–327.
2. T. FUKUSHIMA, S. KURADO and S. KITAHARA, in Proc. 1st Int. Symp. Functionally Gradient Materials, edited by M. Yamanouchi, M. Koizumi, T. Hirai, and I. Shiota, 1990, pp. 145–150.
3. I. SHIOTA, T. SHINOHARA, Y. IMAI and S. IKENO, in Proc. 1st Int. Symp. Functionally Gradient Materials, edited by M. Yamanouchi, M. Koizumi, T. Hirai and I. Shiota, 1990, pp. 219–224.
4. T. HIRAI, M. SASAKI, M. NIINO, *J. JSMS* **36** (1987) 1205–1211.
5. C. KAWAI, S. WAKAMATSU, S. SAKAGAMI and T. IGARASHI, in Proc. 1st Int. Symp. Functionally Gradient Materials, edited by M. Yamanouchi, M. Koizumi, T. Hirai and I. Shiota, 1990, pp. 77–82.
6. M. SASAKI, T. HIRATANI and T. HIRAI, in Proc. 108th Meeting of Japan Inst. Met., 1991, p. 396.
7. M. SASAKI, Y. WANG, T. HIRANO and T. HIRAI, *J. Ceram. Soc. Jpn. Inter. Ed.* **97** (1989) 530–534.
8. M. SASAKI, Y. WANG, A. OKUBO, T. HIRAI, T. HASHIDA and H. TAKAHASHI, *J. Jpn. Soc. Powder and Powder Met.* **37** (1990) 271–274.
9. K. BARMAK, S. W. BANOVIC, C. M. PETRONIS, D. F. SUSAN and A. R. MARDER, *J. Microscopy* **185** (1996) 265–274.
10. N. MERK, X. M. DING and B. ILSCHNER, in Proc. 3rd Inter. Symp. on Structural and Functionally Gradient Materials, edited by B. Ilschner and N. Cherradi (Federal Institute of Technology of Lausanne, Switzerland, 1994) pp. 377–382.
11. X. M. DING, N. MERK and B. ILSCHNER *J. Chin. Soc. Mech. Engr.* **18** (1997) 145–150.
12. B. ILSCHNER, in Proc. 1st Int. Symp. Functionally Gradient Materials, edited by M. Yamanouchi, M. Koizumi, T. Hirai and I. Shiota, 1990, pp. 101–106.
13. K. M. JASIM, R. D. RAWLINGS and D. R. F. WEST, *J. Mater. Sci.* **28** (1993) 2820–2826.
14. V. P. GRECO and W. BALDAUF, *Plating* **55** (1968) 250–257.
15. T. HAYASHI, N. MAEDA and N. FURUKAWA, in Proc. 9th World Congress on Metal Finishing, Amsterdam, 26–29 October 1976, pp. 1–14.
16. M. R. SCANLON, R. R. OBERLE, P. C. SEARSON and R. C. CAMMARATA, in "Mechanical Properties and Deformation Behavior of Materials Having Ultra-Fine Microstructures," edited by M. Nastasi, D. M. Parkin and H. Gleiter (Kluwer Academic Publishers, Boston, MA, 1993) pp. 315–321.
17. M. PUSHPAVANAM, K. BALAKRISHNAN and L. R. SHARMA, *Key Eng. Mater.* **20–28** (1998) 1343–1354.
18. Y. S. CHANG and J. Y. LEE, *Mater. Chem. Phys.* **20** (1988) 309–321.
19. M. VERELST, J. P. BONINO and A. ROUSSET, *Mater. Sci. Eng.* **A135** (1991) 51–57.
20. P. R. WEBB and N. L. ROBERTSON, *J. Electrochem. Soc.* **141** (1994) 669–673.
21. F. K. SAUTTER, *ibid.* **110** (1963) 557–560.
22. S. W. BANOVIC, K. BARMAK and A. R. MARDER, *J. Mater. Sci.* **33**(3) 639–645.
23. S. K. VERMA and H. WILMAN, *J. Phys. D: Appl. Phys.* **4** (1971) 2051–2065.
24. H. K. SRIVASTAVA, *Metal Finishing* May (1995) 20–27.
25. J. A. CROSSLEY, P. A. BROOK and J. W. CUTHBERTSON, *Electrochim. Acta* **11** (1966) 1153–1161.
26. R. BAZZARD and P. J. BOWDEN, *Trans Inst. Met. Finish.* **50** (1972) 63–69.
27. Y. FLOM and R. J. ARSENAULT, *Acta Metall.* **37** (1989) 2413–2423.

Received 9 February 1998
and accepted 22 January 1999